

NEW FOLIC ACID-CHITOSAN DERIVATIVE BASED NANOPARTICLES – POTENTIAL APPLICATIONS IN CANCER THERAPY

LIANA ALUPEI,* GABRIELA LISA,* ANDREEA BUTNARIU,* JACQUES DESBRIERES,** ANCA
NICULINA CADINOIU,*** CATALINA ANISOARA PEPTU,*
GABRIELA CALIN*** and MARCEL POPA*^{****,*****}

*“Gheorghe Asachi” Technical University, Faculty of Chemical Engineering and Protection of the
Environment, Department of Natural and Synthetic Polymers, 73, Prof. D. Mangeron Blvd.,
700050 Iasi, Romania

** Pau et Pays de l'Adour University, IPREM (UMR CNRS 5254), Helioparc Pau Pyrénées,
64053 Pau cedex 09, France

***“Apollonia” University, 2, Muzicii Str., 700399, Iasi, Romania

**** Academy of Romanian Scientists, 54, Independentei Blvd., 50085 Bucharest, Romania

✉ Corresponding author: Marcel Popa, marpopa2001@yahoo.fr

Received April 14, 2016

The active targeting through ligand–receptor-type interactions is exploited for obtaining chitosan-folic acid nanoparticles through double crosslinking reverse emulsion. Stable particles, without toxicity, with sizes appropriate for intravenous administration were prepared. The chitosan derivative was verified by spectral methods (FT-IR, RMN, UV-Vis, XRD) and a thermal technique (TG). The structural characterization of the nanoparticles through FT-IR spectroscopy proved ionic (Na₂SO₄) and covalent (GA) reticulation. The spherical shape, the average diameter and the relatively narrow polydispersity of the nanoparticles were illustrated through SEM, TEM microscopic techniques and laser beam diffractometry. The loading and release capacity was tested using 5-fluorouracil as a model drug, its amount being determined by UV-Vis spectroscopy. The cytotoxicity and hemolysis tests performed on the nanoparticles proved their lack of toxicity and their hemocompatibility. The tests performed on tumor cell lines revealed the capacity of chitosan-folic acid nanoparticles to preferentially bind to these cells, compared to the CS only nanoparticles.

Keywords: chitosan, folic acid, double crosslinking, nanoparticles, 5-fluorouracil, cytotoxicity, hemocompatibility

INTRODUCTION

Cancer incidence has registered an ongoing increase since 1990, when this disease was considered the third cause of death worldwide. In 2012, GLOBOCAN estimated the emergence of approximately 14.1 million new cancer cases and 8.2 million deaths worldwide (approx. 22000 deaths/day). Following the Global Burden of Disease (GBD) studies, the ranking was modified when in 2013 cancer was ranked the second cause of death worldwide after cardiovascular diseases. It is estimated that the number of new cases will reach 21.7 million by 2030, with 13 million deaths as a result of factors such as population growth, aging and the predominance of certain risk factors (smoking, obesity, sedentarism or certain infections).¹⁻³

Presently, the treatment options for the existing cancer types include surgery,

radiotherapy, chemotherapy, immunotherapy, hyperthermia, stem cell transplant – therapies that, although improve the life of the patient, have limitations. In the particular case of chemotherapy, one of the most striking drawbacks is the method's non-specificity when it comes to its action both on the cancer cells and on the normal ones, inducing thus undesired side effects.^{4,5}

Applying nanotechnology in the medicine of cancer is intended to eliminate the drawbacks of the classical treatments. Using nanoparticles with well-studied size, form and surface properties in the cancer therapy has numerous advantages from the point of view of bio-availability, limited solubility, stability, sustained and targeted release, intestinal absorption and therapeutic effectiveness of various drugs.^{6,7}

In order for an antitumor drug to be effective, immediately after being administered it has to be capable to reach the tumor region with a minimum of losses in volume and activity in the blood flow. Also, it has to selectively attack the tumor cells without affecting the normal ones with a controlled release mechanism of the active form.⁸ By means of two ways of targeting, passive and active, the polymer nanoparticles fulfill the conditions imposed by an ideal drug transport system. The wide versatility of the polymer nanoparticles from the point of view of their physical-chemical properties and structure is due to the high variety of monomers/polymers that can be used in obtaining the architectures. Favorable properties, among which, the presence of certain functional groups in the structure, which allow a large array of chemical modifications, biocompatibility, biodegradability and the biomimetic character, justify employing polymers in the drug transport systems.^{9,10}

The strategies for passive targeting based on the enhanced permeability and retention effect (EPR) are explained by the preferential accumulation of the drug transport systems in the tumor area, which is determined by the imperfections of the blood vessels and the weak lymphatic drainage of the tissue. However, recent literature proves that the EPR effect is insufficient for the nanoparticles to penetrate the tumor interstices, thereby the emphasis should be on active targeting.^{11,12} As a means of increasing the recognition of nanoparticles by the target cells, active targeting was applied, where the specific interactions between the drug/its transport system and the target cells are usually described through interactions of ligand-receptor-type.^{13,14} The ligands include carbohydrates, peptides, antibodies or folic acid, which interact exclusively with specific receptors located at the surface of certain types of cells.¹⁵

From the category of markers of surface cells potentially to be used in targeted drug delivery, the receptor of the folic acid stands out as one of the most promising and investigated in the cases of epithelial cancer. Known by the name of "folic acid binding proteins", the folic acid's receptors (FR) are N-glycosylated proteins anchored in the cell membrane, with a great binding affinity for folic acid. These include three glycosyl phosphatidyl inositol isoforms (α , β and γ) with a distribution specific to tissues. While the β isoform is found mainly in myeloid leukemia and the activated macrophages associated to chronic

and autoimmune inflammatory diseases, and the γ form is a soluble protein secreted by the lymphoid cells, the presence of the α isoform is amplified in epithelial cancers (many studies have proved the presence of a very high level, up to 90%, in ovarian cancers).¹⁶⁻¹⁸ It has also been observed that FR is significantly present in some normal epithelia involved in the absorption and retention of folic acid (choroid plexus, placenta, lungs, intestines and kidneys). These are, however, mostly inaccessible to the transport systems administered through blood flow, being localized on apical surfaces of the polarized epithelia; as such, toxicity has not been observed for normal tissues. Other characteristics that recommend using the folic acid as a targeting ligand are the reduced molecular weight (MW = 441 g/mol), stability to various solvents, pH and heat, easy chemical conjugation, lack of immunogenicity and high affinity to its receptor.¹⁹

Chitosan is a linear natural cationic polysaccharide composed of β -(1 \rightarrow 4)-2-acetamido-D-glucose and β -(1 \rightarrow 4)-2-amino-D-glucose units randomly distributed, obtained through the partial deacetylation of chitin (from crustaceous shell) with sodium hydroxide. Chitosan presents three types of functional reactive groups: amino/acetamide, as well as primary and secondary hydroxyl groups from C-6, C-2 and C-3, respectively. Chitosan's solubility depends on the distribution and the number of amino and N-acetyl groups, so that in weak acid solutions (pH < 6.5) the amino groups become protonated, determining the solubilization of macromolecules.

Due to their antitumor, antimicrobial, hypocholesterolemic and immunogenic properties, chitosan presents considerable interest in biomedical applications.²⁰⁻²²

Song *et al.* evaluated the capacity of specific targeting of tumor cells by the chitosan nanoparticles obtained by ionic reticulation with TPP, followed by the conjugation of folic acid at the surface through electrostatic interactions.²³

The aim of this study has been to present a new method for obtaining nanoparticles based on functionalized chitosan with folic acid in order to vectorize them through the targeting ligand towards the folic receptors present on the surface of cancer cells. The novelty of the investigation consists in the crosslinking method (double – both ionic and covalent) in a simple reverse emulsion elaborated by Peptu *et al.*,²⁴ which has the following advantages: the nontoxic ionic

crosslinker, utilized in a major amount, determines the formation of nanoparticles in the first phase, while the minimum amount of covalent crosslinker ensures the required mechanical stability of particles in the intended application without affecting their nontoxic nature – as confirmed in the same study. To the best of the authors' knowledge, this technique is utilized for the first time in obtaining very stable, perfectly defined nanoparticles based on folic acid modified chitosan.

EXPERIMENTAL

Materials

Low molecular weight chitosan (CS, 95% deacetylation degree), folic acid (FA), N-hydroxysuccinimide (NHS), dicyclohexylcarbodiimide (DCC), glutaraldehyde 25% aqueous solution (GA), fluorescein isothiocyanate (FITC), 5-fluorouracil, DMEM and fetal bovine serum were obtained from Sigma Aldrich. 1-ethyl-3-(3-dimethylaminopropyl) carbodiimide (EDC), triethylamine (TEA), Tween 80, Span 80 and hexane were provided by Merck. Acetic acid, toluene, acetone, $\text{Na}_2\text{HPO}_4 \cdot 12\text{H}_2\text{O}$ and $\text{NaH}_2\text{PO}_4 \cdot 2\text{H}_2\text{O}$ came from Chemical Company. Sodium hydroxide (NaOH) and sodium sulfate (Na_2SO_4) were purchased from Lachner, while dry dimethylsulfoxide (DMSO) from Riedel-de Haën. TritonX-100 was received from Scharlau Chemicals. Double distilled water was freshly produced in laboratory. The human blood samples used were freshly obtained from a healthy nonsmoking volunteer. Fibroblast cells were extracted from rabbit dermis in the Bioengineering Department of "Grigore T. Popa" University of Medicine and Pharmacy, Iasi, Romania. GA was first extracted from toluene and then used in the preparation process. The chemicals used in this study were of analytical grade purity and were used without further purification.

Methods

Chitosan-folic acid derivative preparation

In order to obtain the CS derivative with FA, two techniques have been used. The first one obtains the derivative in a single stage, while the second one involves obtaining an intermediate ester of FA with NHS, which, after reacting with CS, will form the derivative. Of the two carboxylic groups present in the structure of the folic acid, α - and γ -, the latter has a much higher reactivity in the condensation reactions with the amino groups mediated by carbodiimides, due to the lower steric hindrance. Recent comparative studies have shown a similar affinity of the folates obtained by chemical reactions at α - and γ - carboxylic groups to folic receptors. This is explained by the fact that receptor binding is performed by means of the pteroyl sequence, while the glutamate group is available for conjugations.^{25,26}

Conjugate preparation through the intermediate FA-NHS ester

The FA-NHS ester was prepared according to a previously reported protocol:²⁷ 0.5 g FA was dissolved in 20 ml dry DMSO, then an excess of 2 moles DCC, NHS and TEA was added to the solution under continuous stirring. The reaction took place overnight, under continuous stirring, in the dark at room temperature. The secondary product (dicyclohexylurea) was removed through filtration, after which the ester was precipitated and washed multiple times with a cold mix of anhydrous ethyl ether containing 30% acetone. The ester was then dried out in vacuum and kept at room temperature.

The next stage in obtaining the CS-FA conjugate proceeded in the following way.²⁸ In an aqueous 1% CS solution in 1% acetic acid (whose pH was raised to 4.5-4.7 by adding a 1M NaOH aqueous solution), a FA-NHS solution in dry DMSO (at a molar ratio CS:FA-NHS = 3:1) was added in fine drops under stirring, the reaction taking place for 16 hours in the dark at 30 °C. At the end of the reaction, the solution was brought to pH = 9 by adding 1M NaOH, the precipitate being dialyzed in phosphate buffer at pH = 7.4 for 3 days and in double distilled water for another 3 days in order to remove the unreacted FA. The polymer was finally freeze-dried.

One-step conjugate preparation

The synthesis of the CS-FA conjugate was based on the method reported in the literature,²⁹⁻³² with a few minor modifications: 0.5 g CS was dissolved in 50 mL aqueous solution 1% acetic acid after which its pH was raised to 4.5-4.7 by adding 1M NaOH. In 20 mL dry DMSO, appropriate quantities of FA (in two molar ratios CS:FA = 3:1 and 1:1) and EDC (molar ratio FA:EDC = 1:2.5) were dissolved, then the solution was added dropwise under stirring over that of CS, the reaction was allowed to proceed for 16 hours in the dark at 30 °C. The reaction was interrupted when 1M NaOH was added to pH = 9 and the precipitate was purified through dialysis in phosphate buffer of pH = 7.4 for 3 days and then in double distilled water for 3 more days. Its isolation was done through freeze-drying. As a result, a yellow sponge-like product was obtained.

Preparation of nanoparticles

An amount of 50 mL CS-FA solution (of desired concentration) was placed in 1% acetic acid aqueous solution, to which the adequate quantity of surfactant, Tween 80, was added in fine drops under constant stirring (Ultraturax, 15.000 rpm) in the organic phase (200 mL toluene containing the proper quantity of surfactant Span 80 perfectly homogenized). After the pre-established time for stabilizing the emulsion, the ionic crosslinking agent solution was added dropwise (Na_2SO_4 5% w/w), the reaction mixture was then transferred to a reactor provided with mechanical

stirrer (500 rpm), where the ionic reticulation continued. After its preset time, the GA solution extracted in toluene ($c = 1.12 \text{ mg/mL}$) was added in drops in order to establish the covalent reticulation process. After the reticulation time was up, the emulsion was broken through centrifugation at 5000 rpm, the particles thus decanted were washed in repeated cycles in double distilled water, acetone and hexane to remove the surfactants and the excess of crosslinking agents. Finally, they were dried in vacuum at $40 \text{ }^\circ\text{C}$. The experimental protocol, including the variable parameters, which has been followed to obtain the nanoparticles, is presented in Table 1.

Characterization techniques

FT-IR spectroscopy

The characterization of the chitosan derivative and the obtained nanoparticles was done from both the spectral and morphological points of view. The new bindings formed in the chitosan derivatives, as well as between the crosslinking agents and the modified polymer in the formation of nanoparticles, were evidenced using two spectrometers BONEM 108B, Canada, and DIGILAB Scimitar FTS 200, USA by the KBr pellet technique.

$^1\text{H-RMN}$ spectroscopy

$^1\text{H-RMN}$ spectra of CS, FA and the CS-FA conjugate were recorded on a Bruker Avance DRX 400 MHz spectrometer in DMSO- d_6 , or D_2O , in which several drops of 1M HCl (up to $\text{pH} \approx 2$) were added, the internal reference being the TMS. The signals obtained were reported in parts per million.

UV-Vis spectroscopy

The degree of transformation of chitosan was evaluated using UV-Vis spectroscopy, considering the folic acid's absorption intensity at 285 nm, on a Nanodrop ND 1000 spectrophotometer. The concentration of the conjugate solution was $2 \times 10^{-2} \text{ mg/mL}$ in 1% acetic acid solution. Previously, a calibration curve was plotted starting from a stock solution of folic acid dissolved in a 0.1M NaOH solution, from which subsequently dilutions were made in the range $0.2\text{-}2 \times 10^{-2} \text{ mg/mL}$ in order to obtain standard solutions necessary to trace the curve. The

equation of the obtained curve was $y = 0.750x + 0.014$, $R^2 = 0.999$.

Thermogravimetric analysis

The thermogravimetric analysis of the conjugate and nanoparticles was accomplished by means of a Mettler Toledo TGA/SDTA 851 system for monitoring mass losses in the destructive process as the temperature increases. The determinations were done in the interval $25 \text{ }^\circ\text{C}\text{-}700 \text{ }^\circ\text{C}$ with a heating speed of $10 \text{ }^\circ\text{C}/\text{min}$, in an inert atmosphere (N_2).

X-ray diffraction

To emphasize the amorphous crystal-like structure and the differences between CS, FA and the conjugate, we used Wide Angle X-ray diffraction (WAXD) on a Bruker AXS D8 Advance diffractometer with a Bragg Brentano goniometer. The scans were registered in pas mode using Ni-filtered radiations with $\text{K}\alpha$, where $\lambda = 0.1541 \text{ nm}$. The working conditions were 40 kV and 30 mA tube power.

Electronic microscopy

Morphological characterization of the nanoparticles was investigated using scanning electron microscopy (SEM) and transmission electron microscopy (TEM) techniques. SEM images were recorded on a HITACHI SU 1510 scanning electronic microscope.

Storing the TEM images was done with a HITACHI HT 7700 microscope, specifically designed for soft materials, operating in high contrast at 100 kV voltage acceleration. The probes were prepared by placing small drops of diluted nanoparticle dispersion ($\sim 1 \text{ g/L}$) on copper grills, of 300 mesh, covered with carbon, then dried in vacuum at $50 \text{ }^\circ\text{C}$.

Determination of particle size

The average diameter of nanoparticles and their dimensional distribution were analyzed by the laser beam diffractometry technique using a SHIMADZU-SALD 7001 diffractometer. All measurements were recorded on nanoparticle suspensions in acetone after their sonication for 10 minutes at room temperature on a Bandelin Sonorex sonication bath. For each probe, three determinations were made.

Table 1
Experimental protocol for obtaining CS-FA based nanoparticles*

Code	Conjugate CS-FA	CS-FA solution conc. (%)	$-\text{NH}_3^+/\text{Na}_2\text{SO}_4$ (mol/mol)	$-\text{NH}_3^+/\text{GA}$ (mol/mol)	Crosslinking time (min)
C_1			1/3.15	1/0.16	
C_2		0.5	1/2.18	1/0.13	
C_3	3:1		1/1.44	1/0.11	
C_4		0.3	1/2.18	1/0.13	
C_5		0.7	1/2.18	1/0.13	
D_1	1:1	0.5	1/3.51	1/0.17	60

* $-\text{NH}_3^+$ represents the quaternary amine groups from the chitosan derivative able to participate at crosslinking

Determining the zeta potential of the particles

In order to assess the stability of the aqueous nanoparticle suspension, the zeta potential (ζ -potential or surface potential) was determined by means of a Delsa Nano C Submicron Particle Size Analyzer (Beckman Coulter). For recording the ζ potential, the device utilizes light electrophoretic diffusion (ELS) by determining the electrophoretic movement of the particles charged in an applied electrical field. The light sources were Dual 30 mW laser diodes at 658 nm. Measurements were done at 25 °C in triplicate, while the analysis mode employed was Smoluchowski.³³

Evaluating the nanoparticles' capacity for drug loading and release

The nanoparticles' capacity for loading and release through diffusion was investigated using 5-fluorouracil (5-FU) as a model drug. The drug is used in the treatment of malignant diseases, such as colorectal, pancreatic, stomach or cervical cancers. As such, a predetermined quantity of dried nanoparticles was immersed in 1.5 mL aqueous solution of 5-FU (10 mg/mL) for 24 h at 30 °C under continuous shaking. After 24 h, the nanoparticle suspension was ultracentrifuged for 15 min at 15000 rpm and freeze-dried. The drug quantity retained in particles was calculated by determining the quantity of 5-FU remaining in the supernatant, using a previously obtained calibration curve, at the wavelength of 265 nm. The equation used was $y = 0.535x$, $R^2 = 0.999$.

The study of the 5-FU release process from nanoparticles was performed as follows. A well-determined quantity of loaded particles was introduced in a dialysis membrane (12000 Da), this being further immersed in 15 mL phosphate buffer solution (pH = 6.7 similar to tumor zones) inside some vials maintained at 37 °C during the entire release process. At pre-established time intervals, the drug quantity released was spectrophotometrically evaluated with the UV-Vis HITACHI U-5100 spectrophotometer, based on the calibration curve of the 5-FU in phosphate buffer at pH = 6.7.

Evaluation of particles' cytotoxicity

Cell viability has been estimated by the MTT [3-(4,5-Dimethylthiazole-2-yl)-2, 5-diphenyl tetrazolium] test, which represents a quantitative colorimetric method relying on splitting the tetrazolium salt (yellow) and forming insoluble formazan crystals (purple), by the mitochondrial dehydrogenases of viable cells. Beforehand, nanoparticles were sterilized through UV radiation for 24 h. A number of 10000 of fibroblast cells were placed in 3 24-well plates (one plate each day). The medium in which they were cultivated was DMEM, supplemented with 10% fetal bovine serum and 1% antibiotics (mix of penicillin, streptomycin, neomycin). Subsequently, volumes of suspensions of the concentrations to be tested (50 and 100 $\mu\text{g/mL}$) were added onto the cells, so that the final

volume of the mix was 500 $\mu\text{L/well}$. In each plate, three control wells were left (over which no particle suspension was added) and three wells for each suspension to be analyzed. We used one plate for each evaluation (24 h, 48 h, 72 h). After each of the three time intervals, the culture medium and the nanoparticles from the control and the analyzed cells were removed and a solution of 5% MTT [3-(4,5-Dimethylthiazole-2-yl)-2,5-diphenyl tetrazolium] was added; then the plate was left in the incubator for 2 hours (37 °C, CO₂ 5% and 95% humidity) in the dark. After 2 h, the MTT solution was removed from the wells and isopropanol was added, the formed crystals were left to be solubilized for 20 min under shaking. We then collected 100 μL from each probe and read out the absorbance for both the control and the analyzed probes at 570 nm. To this end, we used a TECAN plate reader. From the determined absorbance, we subtracted the plate noise. We considered that the control cells presented 100% viability. The computation of the tested probes' viability was done on the basis of the ratio:

$$\text{Viability (\%)} = \text{Abs}_{\text{test}}/\text{Abs}_{\text{control}} * 100 \quad (1)$$

where Abs are the absorbances for the tested and control probes, respectively.

Evaluation of particles' hemocompatibility

Hemolysis experiments were performed using a method adapted from Vuddanda *et al.*³⁴ The human blood sample used was freshly obtained from a healthy nonsmoking volunteer, following the proper institutional ethical procedure and with an informed consent. First, 5 mL blood was centrifuged at 2000 rpm for 5 min. The surface layer of the supernatant plasma was removed and the red blood cells (RBC) were separated and washed several times with a normal saline solution. Then, the purified RBC was resuspended in a normal saline solution to obtain 25 ml of RBC suspension. 2 ml of NP suspension in the normal saline solution at different concentrations were added to 2 mL of RBC suspension (final concentrations were 100 $\mu\text{g NP/ml}$, 200 $\mu\text{g NP/ml}$ and 400 $\mu\text{g NP/ml}$). Positive (100% lysis) and negative (0% lysis) control samples were prepared by adding equal volumes of Triton X-100 2% and normal saline solution, respectively, to the RBC suspension. The samples were incubated at 37 °C for 2, 4 and 6 h. The samples were slightly shaken once every 30 min to resuspend the RBC and NP. After the incubation time, the samples were centrifuged at 2000 rpm for 5 min and 1.5 mL of supernatant was incubated for 30 min at room temperature to allow hemoglobin oxidation. Oxyhemoglobin absorbance in supernatants was measured spectrophotometrically (PG Instruments T60 UV-Vis Spectrophotometer) at 540 nm. Hemolysis percentages of the RBC were calculated using the following formula:

$$\% \text{Hemolysis} = (\text{Abs}_{\text{sample}} - \text{Abs}_{\text{negative control}}) / (\text{Abs}_{\text{positive control}} - \text{Abs}_{\text{negative control}}) \quad (2)$$

The experiments were performed in triplicate.

Cytofluorimetric analysis

The aim of this analysis was to emphasize the biodistribution of the nanoparticles based on chitosan, native and modified, at the level of tumor cells, after being administered. Nanoparticles were previously labeled with fluorescein, after their preparation, in accordance with the protocol presented by Chekina *et al.*³⁵ Fluorescein labeling was based on the reaction between FITC's isothiocyanate group and the primary amino group from the particles' surface with the formation of a thiourea bond. 3 mg of FITC in an acetone/water mixture (0.3/2.7, v/v) was added in 10 mL nanoparticle dispersion (native and to be tested) of 1 mg/mL concentration, in pH = 7.4 phosphate buffer. The reaction took place for 12 h at 23 °C in the dark. Finally, the nanoparticles were washed with phosphate buffer (pH = 7.4) in order to remove the non-conjugated FITC.

We used tumor cells of type A549, whose culture medium was DMEM + 10% fetal bovine serum + 2 mM L-glutamine + 100 units/ml penicillin + 100 µg/ml streptomycin + 5% CO₂ at 37 °C. Two types of fluorescein labeled nanoparticles were used: double crosslinked CS-based nanoparticles (native) and double crosslinked CS-FA-based ones (to be analyzed). As such, 5.000 cells/ml of medium, treated with the two types of nanoparticles fluorescently labeled, were administered in concentration of 1% in the cells' culture medium, for 48 hours.

Highlighting the labeled particles was done through cytofluorimetric analysis performed 48 h after the incubation of the tumor cells with native or analyzed nanoparticles. After washing twice with phosphate buffer and centrifuging, the cells treated with nanoparticles and the native ones were resuspended in 1 mL phosphate buffer and analyzed by the cytofluorimetric method, using a Becton Dickinson flow cytometer of type FACS CaliburTM.

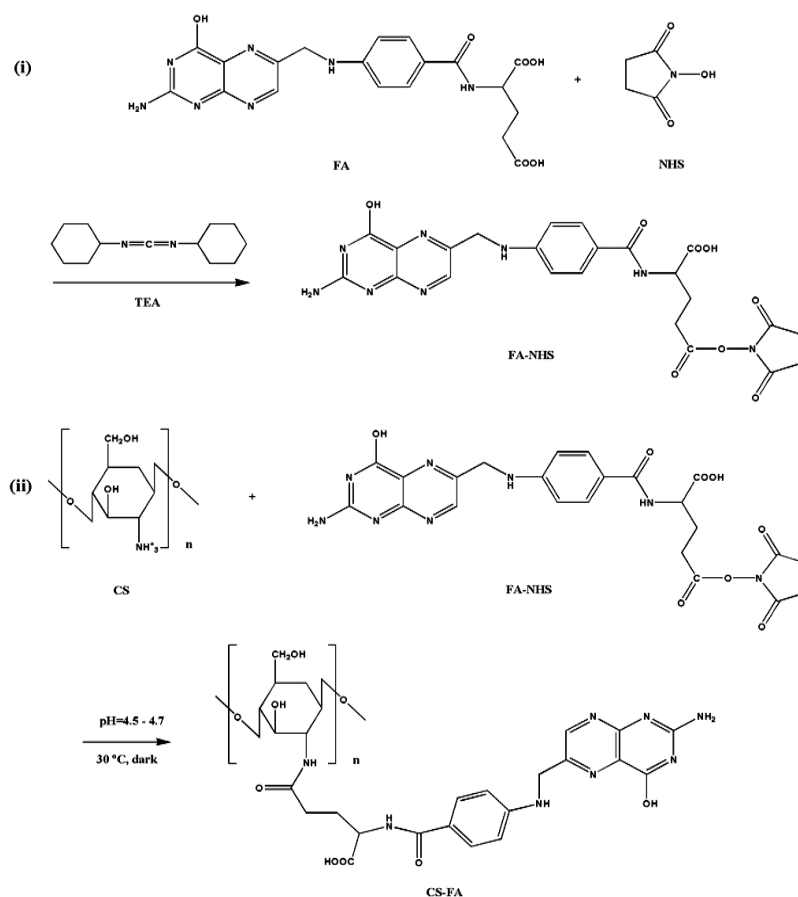


Figure 1: Schematic representation of conjugate preparation through FA-NHS intermediate ester; (i) first step: synthesis of intermediate ester of folic acid with N-hydroxysuccinimide (FA-NHS); (ii) second step: reaction between chitosan and folic acid ester leading to chitosan-folic acid conjugate (CS-FA)

RESULTS AND DISCUSSION

The present work aimed to obtain new nanoparticles capable of an active targeting of antitumor drugs to tumor cells, relying on a method previously developed by our group.²³ The method is based on the double crosslinking of chitosan, previously modified with folic acid (by means of an amidic bond) in order to obtain stable particles, devoid of toxicity, capable of being directed towards the target cells possessing folic receptors. The technique involves a first ionic reticulation of the chitosan derivative by means of Na_2SO_4 , followed by the mechanical stabilization of the already formed particles by a minimum covalent reticulation through the GA, both reactions taking place at the free amine groups of the chitosan derivative. By adjusting certain

parameters of the process, the method allows to obtain submicronic particles suitable for the intended applications, namely their intravenous administration.

CS-FA conjugate preparation

In order to obtain the chitosan derivative with folic acid, two methods were employed. The first one involves the preparation of folic acid-modified chitosan in two steps (Fig. 1). Foremost, the synthesis of the intermediate folic acid-N-hydroxysuccinimide ester (FA-NHS) was performed, followed by the reaction between chitosan and FA-NHS, resulting in CS-FA formation.

The second method represents the one-step formation of the CS-FA conjugate (Fig. 2).

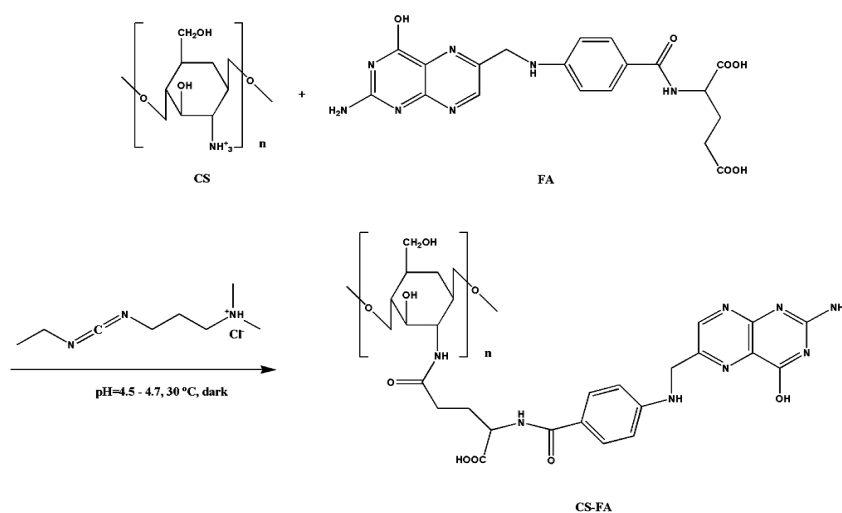


Figure 2: Schematic representation of one-step conjugate preparation (CS-FA)

The spectral analysis performed on the derivatives obtained by the two previously described methods (at a molar ratio of CS:FA-NHS = 3:1 and CS:FA = 3:1) showed no significant differences, while the degree of substitution determined through the UV-VIS spectrophotometrical method reveals very similar values. Therefore, in the production of the nanoparticles, we decided that it is more convenient to synthesize the chitosan derivative in one step considering reasons such as saving time and reagents.

FT-IR analysis of CS-FA

The qualitative proof of functionalizing the chitosan with folic acid consists in the comparative FT-IR spectra of the departing

compounds and of chitosan derivatives in the two molar ratios $-\text{NH}_3^+/\text{FA}$ (Fig. 3).

The FT-IR spectra present similar profiles for both CS and FA, so that the majority of the absorption bands overlap. However, in the case of the two derivatives (3:1 and 1:1 compounds), one notices a slight shift of the absorption bands. Also, comparing to the simple chitosan spectra, the spectra of the two derivatives present new bands at the wavenumbers 1510 cm^{-1} and 1560 cm^{-1} for probes 3:1 and 1:1, respectively. These signals are specific to the vibrations of the C=C bonds from the aromatic ring present in the structure of the folic acid.³⁶⁻⁴⁰

¹H NMR spectroscopy

The characterization of the conjugates through ¹H NMR spectroscopy reveals the fact that their

at a heating speed of 10 °C/min, are represented in Figure 5. From the chitosan's DTG curve, we can detect two weight loss stages: the first one reaches T_{peak} at approximately 52 °C, is accompanied by a mass loss of 9.7% (endothermic process) and is attributed to the water evaporation from the polymer. The second stage begins at approximately 267 °C and ends at

430 °C, being associated with a mass loss of 52.94%, determined by the loss of the volatile compounds resulted in the thermal degradation of the polymer chain. Polysaccharide pyrolysis starts with the random break of the glycosidic bonds, followed by a decomposition that forms acetic and butyric acids, along with a series of inferior fatty acids.⁴²

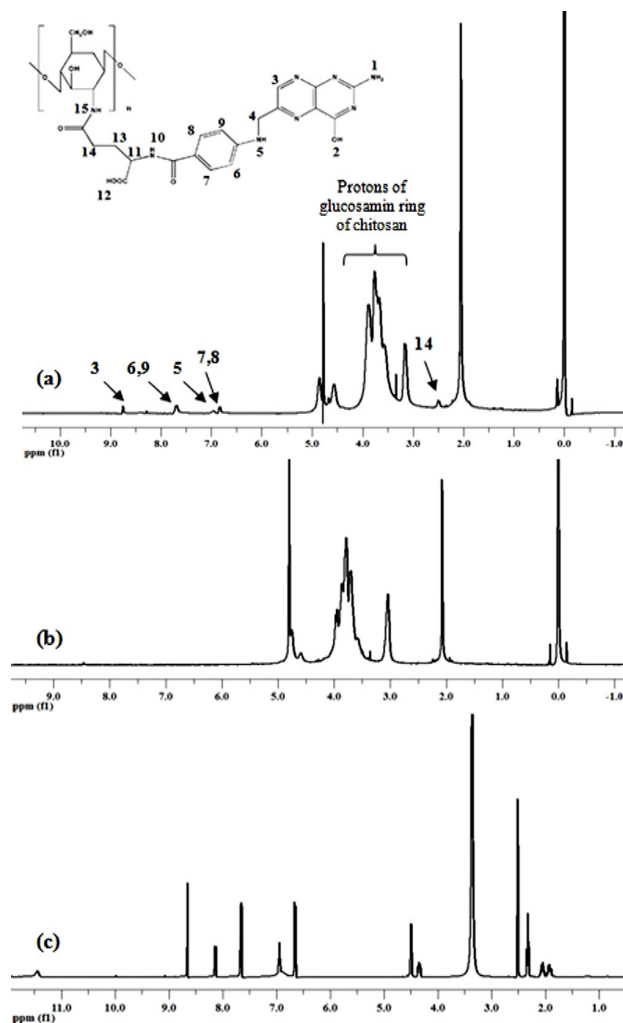


Figure 4: ¹H NMR spectra of (a) CS-FA (CS:FA = 3:1 molar ratio), (b) CS, (c) FA

The folic acid is less thermally stable, beginning to decompose at 117.8 °C with a mass loss of 5.82%; more intense degradation appears in the interval 235.27-333.8 °C, when the probe loses 21.97% of its weight. Of note is that it registers the highest value of the residue upon decomposition at the temperature of 700 °C.

As one can notice, the form of the derivatives' DTG curves resembles the ones for chitosan, but suggesting an inferior thermal stability. The main

degradation steps occur in the intervals 249-306 °C with a mass loss of 39.73%, and respectively, 247-338 °C with mass loss of 52.08%. The difference occurs in the case of the molar ratio 1:1, where one can see a supplementary degradation step over the temperature of 487 °C, associated with a loss of 43.39%, explained by the presence of a larger quantity of folic acid bound to chitosan. We see that with the increasing of the FA amount, the degradation temperature of the

derivative decreases. Therefore, the derivative with a higher degree of substitution will degrade at lower temperatures, given the inferior thermal

stability of the folic acid compared to that of the chitosan.

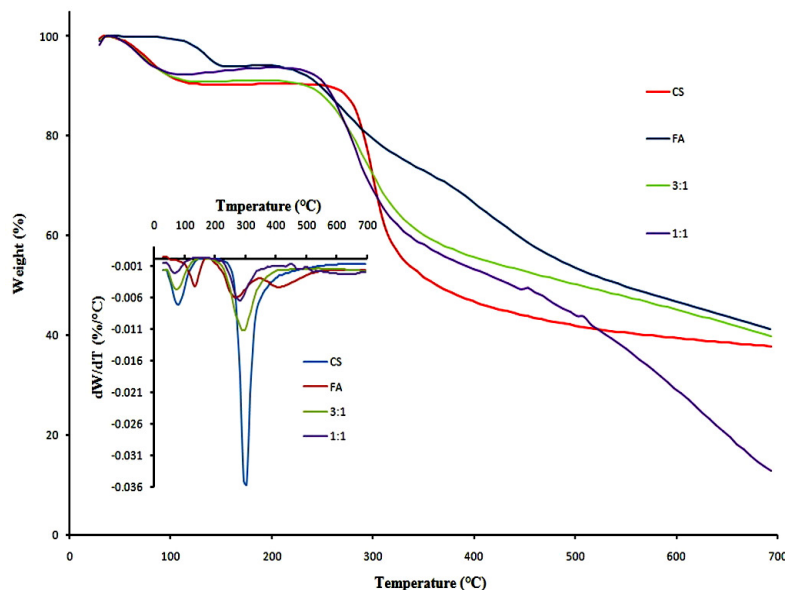


Figure 5: TG and DTG curves of CS, FA and derivatives 3:1 and 1:1

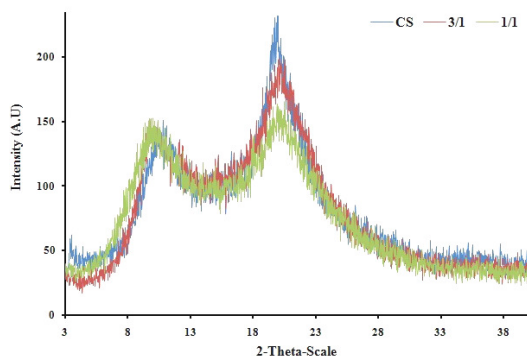


Figure 6: XRD diffractograms of native CS, 3:1 and 1:1 molar ratio derivatives

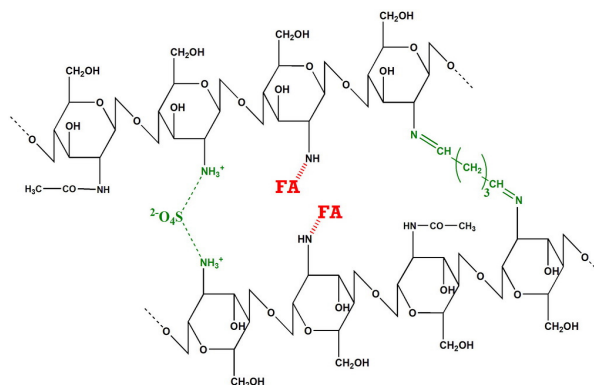


Figure 7: Schematic representation of ionic crosslinking (Na_2SO_4) and covalent crosslinking (GA) reactions of the conjugate in the formation of nanoparticles; FA – folic acid conjugated to chitosan

XRD analysis

X-ray spectroscopy also allowed gaining indirect information regarding the attainment of chitosan. Chitosan is a semi-crystalline polymer, the corresponding diffractogram presenting high intensity characteristic peaks at $2\theta = 10.42$ and 19.83 (Fig. 6). Folic acid is also a crystallizable compound, which presents a diffractogram with characteristic high intensity peaks at $2\theta = 5.43$ and 19.83 , and of lower intensity at $2\theta = 13.1$ and 16.38 . The diffractograms corresponding to the

two derivatives, characterized by different degrees of substitution resemble that of the chitosan, but with a slight shift of the high intensity peaks, along with the modification of their ratio.

Comparing the two derivatives' diffractograms, one notices a slight increase in peak intensity at $2\theta = 9.95$ in the case of the derivative with the higher degree of conversion (CS:FA = 1:1 molar ratio). This is due to the contribution of folic acid, which is in a higher

proportion than in the case of the 3:1 compound. In addition, compound 1:1 shows a slight shift towards lower values of 2θ , obviously due to the same causes. Accordingly, chitosan's characteristic peak decreases in intensity as an

effect of the decrease in weight of the polysaccharide in the derivative composition. In our opinion, the obtained result constitutes an indirect qualitative proof of the fact that the polysaccharide has been successfully modified.

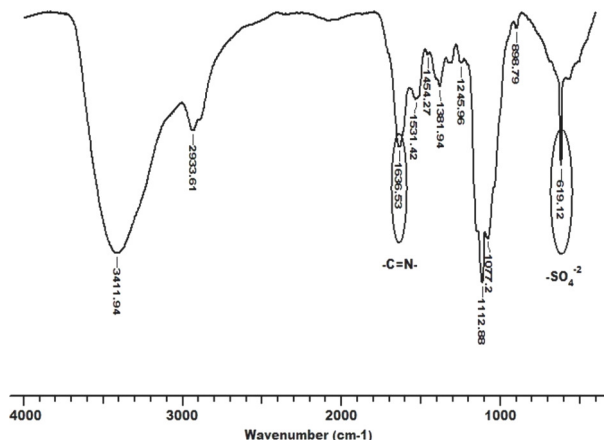


Figure 8: FT-IR spectra of C_1 nanoparticles

Preparation of nanoparticles

Particles based on the CS-FA conjugate were mentioned before in the literature,^{28-30,32,43} but the novelty of our research is constituted by the obtaining method, namely double reticulation in reverse emulsion, the formed structure being schematically represented in Figure 7.

The two stages of the reticulation process are essential in the formation of the nanoparticles: the ionic interactions (for a first build of nanoparticles by ionic gelation) and the covalent reactions (to increase the mechanical and dimensional stability of the particles). Both crosslinking agents, bifunctional, create bridges with the ammonium/amine groups of the conjugate. The GA, being very reactive even at moderate temperatures, accomplishes stable iminic bonds.

Spectral characterization of nanoparticles

The FT-IR spectra recorded for all types of nanoparticles confirm the fulfillment of the two types of reactions. We chose the FT-IR spectrum of probe C_1 as a representative example (Fig. 8). The absorption bands specific to the iminic bonds $-C=N-$ resulted after the covalent reticulation are present at 1636.5 cm^{-1} . The absorption band from 619.1 cm^{-1} is attributed to the ionic reticulation bond established between the sulfate anion from Na_2SO_4 and ammonium cation of the conjugate.

Thermogravimetric analysis of nanoparticles

Given the chemical transformations undergone by the conjugate, following reticulation, we considered useful to investigate the thermal behavior of nanoparticles, starting from the idea of their possible thermal sterilization. Surprisingly, the derivative based particles present a thermostability slightly inferior to that of the modified polymer from which they were obtained. A possible explanation would be the degradation of the bridges established by the $-\text{SO}_4^{2-}$, through ionic bonds. According to the mass loss curves from Figure 9, the degradation process of nanoparticles takes place in 5 stages, as opposed to that of the derivative discussed above, which required 3 stages. The first two stages ranging between $62.22\text{--}214\text{ }^\circ\text{C}$, associated with a mass loss of 24.6%, are determined by the water elimination and the loss of the volatile compounds. The residue produced in the thermal degradation process is 34.8%. The main degradation stage, the third one, from $271.5\text{--}339.4\text{ }^\circ\text{C}$, with a loss of 23.6%, corresponds to the polymer's degradation, as in the case of the derivative.

Morphological and dimensional analyses of the nanoparticles

The morphological characteristics of nanoparticles have been examined by electronic

microscopy (SEM and TEM). As can be seen from Figures 10 and 11, the particles have a spherical form and different agglomeration tendency, with diameters ranging between 100-350 nm. In accordance with the experimental protocol (Table 1), the varied parameters in obtaining the nanoparticles led to morphological differences, as observed in the SEM and TEM images. For the set of probes C₁-C₃, the concentration of the polymer solution was maintained constant (0.5%), modifying the molar ratio NH₃⁺/crosslinking agent. Actually, with the decrease of the crosslinking agent quantity, we notice an increase in the agglomeration tendency, explained by the crosslinking density decrease of the polymer matrix (C₃). In the case of the probes C₂, C₄, C₅, in which the polymer/crosslinking agent ratio was kept constant, modifying the concentration of the polymer solution led to the following observation. The diameter of the particles grows with the polymer solution concentration, being larger for the probe C₅, an

effect which was reported in previous works.⁴⁴ For more diluted solutions (C₄), the form of the particles is not as well-delineated any more, as a consequence of a weaker reticulation. In the case of C₅ particles, where the concentration of the solution rose to 0.7%, we notice a slight increase in polydispersity and a decrease in the agglomeration tendency. Between C₁ and D₁ particles, for which we used the same solution concentration and volume of crosslinking agent solution, we remark a slight increase in the average diameter of D₁ particles. This fact could be explained by the higher value of substitution degree of CS, which determines a slight reduction of the amino groups that can participate in reticulation, and thus the decrease of the reticulation density of particles with consequences over their diameter.

The diameter of the particles, as it is revealed in the TEM images, is in good agreement with that illustrated by the SEM images.

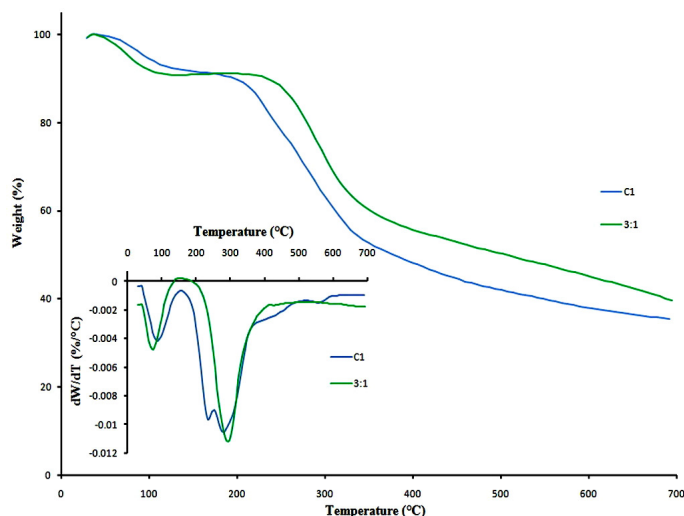


Figure 9: TG and DTG curves of 3:1 derivative and C₁ nanoparticles

Dimensional analysis and stability of nanoparticles

The differential curves of the granulometric distribution manifest a monomodal aspect, with a relatively narrow polydispersity, the average diameter of the nanoparticles being presented in Table 2.

The particle size measurements were made in acetone in order to limit their swelling (which occurs in water), and thereby to have a picture of the size and shape close to that in dry state. The results are in full agreement with those obtained

from SEM and TEM images, illustrating once again the fact that the size and polydispersity of the particles are in close relation with the amino groups/crosslinking agent ratio. The reduction of the particle diameter, as a consequence of a higher crosslinking density, is more and more pronounced as the NH₃⁺/crosslinking agent ratio decreases, resulting in smaller and more individualized particles.

To exemplify, Figure 12 shows the dimensional polydispersity curves for the probes C₁ and C₃.

The zeta potential (Table 2) was determined in order to investigate the state of the particles' surface and to predict the stability of their aqueous suspensions over time. Higher values indicate the fact that the repulsion forces are larger and the system becomes more stable. When the potential is low, attraction exceeds repulsion and the dispersion will flocculate. According to the literature, values of ζ potential between ± 10 and ± 30 mV determine an incipient instability of the particles.⁴⁵

The stability of the suspensions rises (zeta potential rises) as the crosslinking agent quantity is lower, given that there remain more free amine groups that determine more intense repulsion forces between particles.

Nanoparticles capacity for loading and release of 5-FU

The morphological and dimensional analyses proved that the best features for the specific application (well-defined form, smallest average diameter, relatively narrow polydispersity, increased zeta potential) belong to C_1 type nanoparticles. Even though zeta potential is slightly lower than for C_2 and C_5 samples, C_1 presents a good dispersion. Moreover, drug loading tests confirmed that the amounts of drug retained by the other samples were slightly lower than for sample C_1 .

For the loading and release studies, we chose probe C_1 as the representative that retained a drug quantity of 137.8 mg 5-FU/g nanoparticles. The

probe was tested from the point of view of the capacity of *in vitro* release, the kinetics of release in a lightly aqueous acid medium (pH = 6.7) being shown in Figure 13. The behavior upon release is typical of diffusional systems, presenting not a very pronounced characteristic "burst effect", followed by a slower release stage. The first stage of the release process is determined, obviously, by the release of the drug molecules adsorbed onto the surface of the nanoparticles, which takes place in the first hour of the process. Slow kinetics is established afterwards, typical of diffusional systems. After 230 h, the quantity of 5-FU released from nanoparticles reaches approx. 60 mg/g particles, and they still manifest the tendency to release the drug afterwards.

The analysis of the release kinetics of 5-FU from probe C_1 was performed on the basis of the mathematical model Korsmeyer-Peppas.^{46,47}

$$y = 0.803x - 2.229, R^2 = 0.961 \quad (3)$$

It is known from the literature that the factors affecting drug release kinetics from a hydrophobic matrix include tortuosity, porosity, diffusion coefficient, solubility *etc.*⁴⁸ The preparation of the experimental kinetic data in the interval 0-200 minutes allowed to calculate the diffusional exponent as being $n = 0.803$. This value ($0.5 < n < 1.0$) suggests an abnormal diffusion, non-Fickian, the process of drug transport through the polymer matrix being governed both by diffusion and swelling of the polymer network.⁴⁹⁻⁵¹

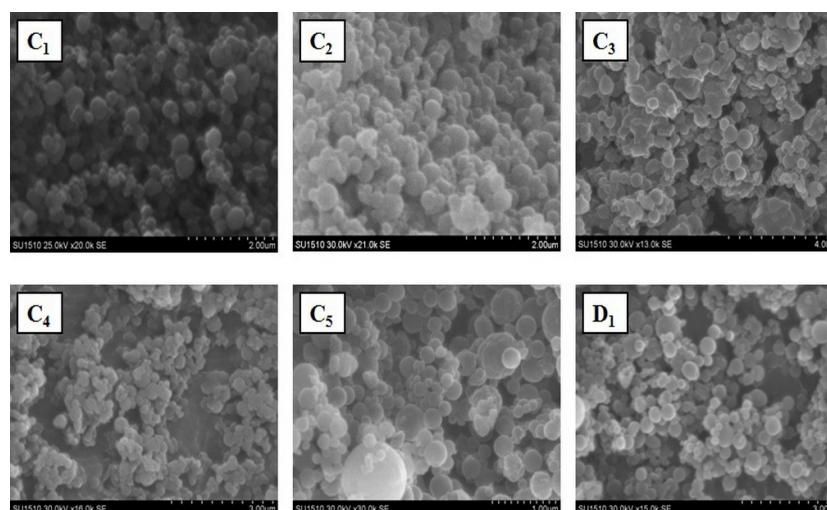


Figure 10: Scanning electron microscopy images of C_1 , C_2 , C_3 , C_4 , C_5 , D_1 probes

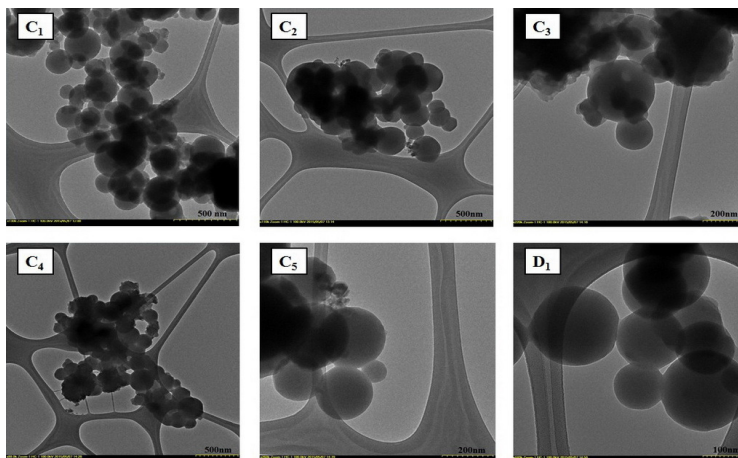


Figure 11: Transmission electron microscopy images of C₁, C₂, C₃, C₄, C₅, D₁ probes

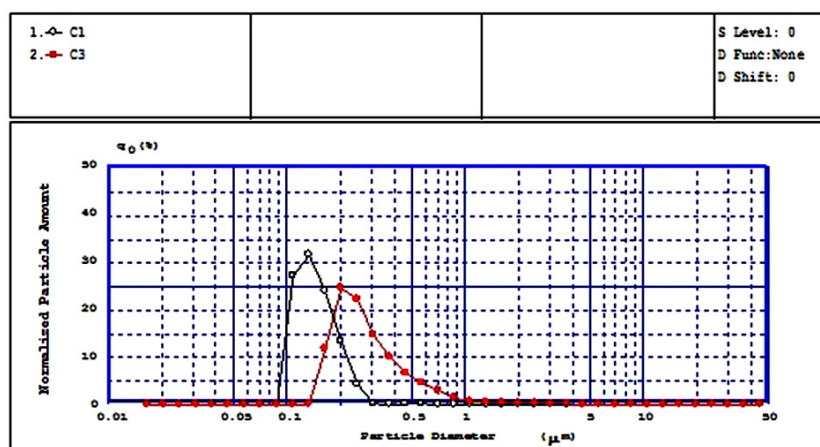


Figure 12: Dimensional polydispersity curves of CS-FA nanoparticles determined by laser diffractometry for C₁ and C₃

Table 2
Zeta potential values and average diameter for the obtained nanoparticles

Code	Zeta potential (mV)	Mean diameter (nm)		
		SEM	TEM	SALD
C ₁	+13.07	150 – 200	100 – 200	167
C ₂	+18.78	200 – 250	150 – 250	214
C ₃	+16.58	250 – 300	250	317
C ₄	+14.26	250 – 300	250	361
C ₅	+16.73	300	250 – 300	289
D ₁	+11.74	250	250	221

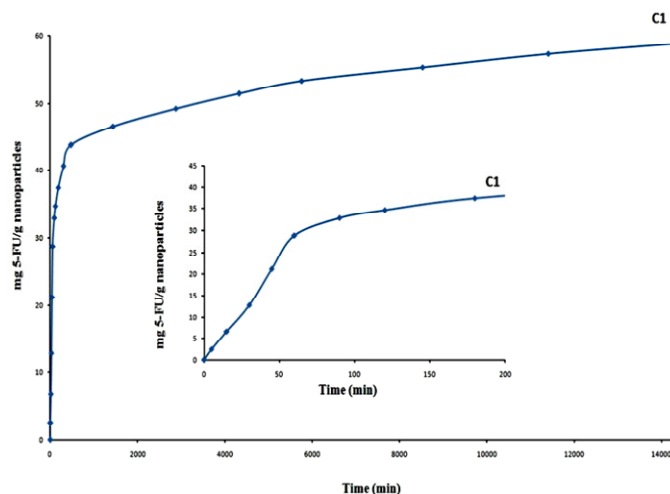


Figure 13: Release kinetics curve of 5-FU from C₁ sample (phosphate buffer, pH = 6.7, 37 °C)

Cytotoxicity

Determining cell viability is one of the most common analyses in the cytotoxicity evaluation of biomaterials. In general, cell viability values of synthesized particles rank at high levels. As an example, Figure 14 shows such values for the particles C₁ and C₅. The toxicity test was accomplished at two different concentrations of the suspension: 50 µg/mL and 100 µg/mL. The UV absorbance was read out at 24, 48 and 72 h, the tests being performed in triplicate. Even though sample C₅ has the highest values of viability, one remarks that sample C₁ presents nearby values. The values registered for the two concentrations listed in Figure 14 confirm that the analyzed particles may be included in the category of those lacking toxicity.⁵²

Hemolysis

Hemolysis represents the disintegration of red blood cells with the release of hemoglobin and other internal components into the surrounding fluid. If this disintegration occurs to a significant number of red blood cells in the body, it can lead to dangerous pathological conditions. Therefore, all biomedical products designed to be administered intravenously must be evaluated for their hemolytic potential.⁵³ Since the obtained nanoparticles can be used as drug delivery systems and can be administered intravenously, preliminary tests on their interaction with human blood components were necessary. Chitosan-based nanoparticles obtained by different methods, with sizes ranging between 200 and 400 nm and positively charged, are hemocompatible for concentrations less than 50 µg/mL, as

demonstrated in the literature.^{54,55} The hemolytic potential of chitosan-folic acid nanoparticles was evaluated for concentrations between 100 and 400 µg/mL, using a spectrophotometric method. The results of the hemolysis assay are shown in Figure 15. The results were expressed as means ± SD (n = 3).

Figure 15 comparatively shows the values for the samples that registered the lowest hemolytic potential, namely C₁ and C₁. Sample C₃ was chosen as a reference due to its smallest hemolysis percentage. With respect to it, sample C₁ has similar values, which supports once again the choice of sample C₁ in performing all of the tests presented in our work.

It was observed that the hemolytic percentage increases with the increasing of nanoparticles concentration. A sample is considered as hemolytic if the hemolytic percentage is above 5%.⁵⁶ It is evident from the graph (Fig. 15) that the hemolytic percentage was lower than 5% only for two tested concentrations (100 µg/mL and 200 µg/mL), in all three test runs. However, a concentration of 400 µg nanoparticles per mL produced a hemolytic percentage above 5%, in all three test runs. The haemolysis results revealed that the tested nanoparticles were suitable for systemic administration if their concentration in the bloodstream is lower than 200 µg/mL.

Cytofluorimetric analysis

The obtaining of chitosan-folic acid-based nanoparticles aimed at accomplishing their active targeting towards tumor cells, whose receptors are capable of recognizing certain ligands, among which the folic acid. In order to test the

nanoparticles' capacity to attach to tumor cells, to a greater extent than the ones from unmodified CS, an experiment was devised consisting in placing them (C_5 probe) on a culture of tumor

cells, evaluating the degree to which they orient towards the cells, in comparison with the simple CS particles. The resulting histograms are presented in Figure 16.

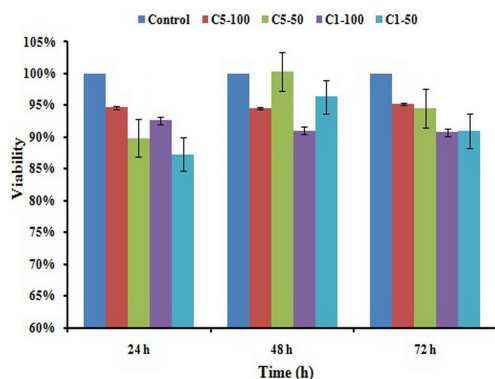


Figure 14: Cellular viability for samples C_1 and C_5 at 50 $\mu\text{g/mL}$ and 100 $\mu\text{g/mL}$ concentrations

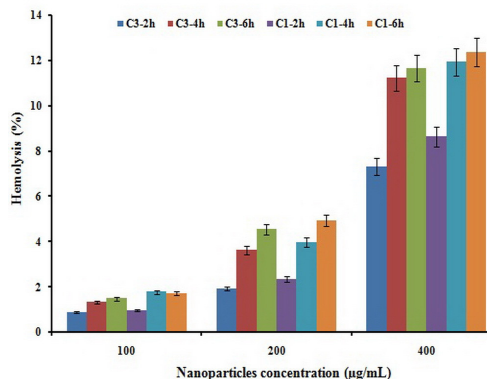


Figure 15: Hemolysis percentage after 2, 4 and 6 hours of exposure to C_1 and C_3 nanoparticles

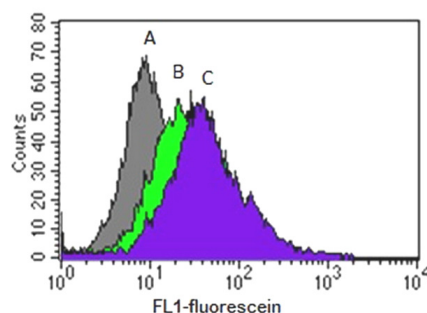


Figure 16: Representative fluorescence histograms for A549 cells. Control (A), cells exposed for 48 h to CS fluorescein labeled nanoparticles (B) and cells exposed for 48 h to C_5 fluorescein labeled nanoparticles (C)

We find that the CS-FA nanoparticles, fluorescently labeled, are intercepted in a greater proportion (by approx. 26% more) by the tumor cells, after 48 h of incubation. The experiment demonstrates that the goal of our research has been reached, in the sense that the chitosan particles functionalized with folic acid have a higher capacity to orient and fasten to the walls of tumor cells.

In conclusion, this type of nanoparticles could be used as an effective system for drug targeting.

CONCLUSION

In the present work, we obtained a chitosan derivative by chemical modification with folic acid, using two synthesis techniques (in one step and two steps) that led to compounds with similar degrees of substitution (in the case of CS:FA-NHS = 3:1 and CS:FA = 3:1 molar ratio), as

determined by UV-Vis spectroscopy. Thereby – for reasons of saving time and reactivities – the one-step method proved to be more convenient. We obtained, for the first time, nanoparticles based on a chitosan derivative with folic acid, by means of the double crosslinking method (ionic and covalent) in a reverse emulsion, with the goal of being tested as carriers of a cytostatic drug towards the target (tumor cells). The morphological characteristics of the nanoparticles (diameter, dimensional polydispersity) depend on the quantity of crosslinking agent used and on the substitution degree of chitosan. The resulted nanoparticles are biocompatible, which is confirmed by their lack of toxicity (cell viability is high in their presence) and hemocompatible (for concentrations of the aqueous suspensions lower than 200 $\mu\text{g/mL}$). The values of the zeta potential between +11.75 and +18.78 mV ensure

good dispersability, an essential property for applications involving the administration through intravenous injection. The nanoparticles have the capacity of loading and sustained release of 5-fluorouracil, which makes them potentially utilizable in cancer therapy, given also their capability of being recognized by the tumor cell folic receptors, as proven by the cytofluorimetric analysis.

REFERENCES

- ¹ M. Naghavi, *JAMA Oncol.*, **505**, 1 (2015).
- ² L. A. Torre, F. Bray, R. L. Siegel, J. Ferlay, J. Lotet-Tieulent *et al.*, *CA Cancer J. Clin.*, **87**, 65 (2015).
- ³ “Global Cancer Facts and Figures”, 3rd ed., American Cancer Society, Inc., No. 861815, 2015, pp. 1-61.
- ⁴ K. T. Nguyen, *J. Nanomedic. Nanotechnol.*, **1**, 2 (2011).
- ⁵ A. Urruticoechea, R. Alemany, J. Balart, A. Villaneuva, F. Vinlas *et al.*, *Curr. Pharm. Des.*, **3**, 16 (2010).
- ⁶ M. R. Diaz and P. E. Vivas-Mejia, *Pharmaceuticals*, **6**, 1361 (2013).
- ⁷ T. Sun, Y. S. Zhang, B. Pang, D. C. Hyun, M. Yang *et al.*, *Angew. Chem. Int. Ed.*, **53**, 12320 (2014).
- ⁸ K. Cho, X. Wang, S. Nie, Z. G. Chen and D. M. Shin, *Clin. Cancer Res.*, **14**, 1310 (2008).
- ⁹ K. Shroff and A. Vidyasagar, *J. Phys. Chem. Biophys.*, **1**, 3 (2013).
- ¹⁰ D. Bennet and S. Kim, in “Application of Nanotechnology in Drug Delivery”, edited by Ali Demir Sezer, InTech, 2014, pp. 257-310.
- ¹¹ N. Bertrand, J. Wu, X. Xu, N. Kamaly and O. C. Farokhzad, *Adv. Drug Deliv. Rev.*, **2**, 66 (2014).
- ¹² D. S. Spencer, A. S. Puranik and N. A. Peppas, *Curr. Opin. Chem. Eng.*, **84**, 7 (2015).
- ¹³ S. M. Sagnella, J. A. McCarroll and M. Kavallaris, *Nanomed. Nanotech. Biol. Med.*, **10**, 1131 (2014).
- ¹⁴ Y. H. Bae and K. Park, *J. Control. Release*, **198**, 153 (2011).
- ¹⁵ V. K. Khanna, *ISRN Pharmacol.*, **1**, 2012 (2012).
- ¹⁶ X. Zhao, H. Li and R. J. Lee, *Expert Opin. Drug Deliv.*, **309**, 5 (2008).
- ¹⁷ R. J. Lutz, *Transl. Cancer Res.*, **118**, 4 (2015).
- ¹⁸ C. Marchetti, I. Palaia, M. Giorgini, C. De Medici, R. Iadarola *et al.*, *Oncol. Targets Ther.*, **7**, 1223 (2014).
- ¹⁹ A. R. Hilgenbrink and P. S. Low, *J. Pharm. Sci.*, **94**, 2135 (2005).
- ²⁰ J. Zhang, W. Xia, P. Liu, Q. Cheng, T. Tahirou *et al.*, *Mar. Drugs*, **8**, 1962 (2010).
- ²¹ M.-C. Chen, F.-L. Mi, Z.-X. Liao and H.-W. Sung, *Adv. Polym. Sci.*, **185**, 243 (2011).
- ²² E. Bobu, R. Nicu, M. Lupei, F. Ciolacu and J. Desbrieres, *Cellulose Chem. Technol.*, **45**, 619 (2011).
- ²³ H. Song, C. Su, W. Cui, B. Zhu, L. Liu *et al.*, *Biomed. Res. Int.*, **1**, 2013 (2013).
- ²⁴ C. A. Peptu, G. Buhus, M. Popa, A. Perichaud and D. Costin, *J. Bioact. Compat. Polym.*, **98**, 25, (2010).
- ²⁵ S. D. Boss, T. Betzel, C. Muller, C. R. Fischer, S. Haller *et al.*, *Bioconjugate Chem.*, **74**, 27 (2016).
- ²⁶ C. Chen, J. Ke, X. E. Zhou, W. Yi, J. S. Brunzelle *et al.*, *Nature*, **486**, 500 (2013).
- ²⁷ R. J. Lee and P. S. Low, *J. Biol. Chem.*, **269**, 3198 (1994).
- ²⁸ J. Ji, D. Wu, L. Liu, J. Chen and Y. Xu, *Polym. Bull.*, **68**, 1707 (2012).
- ²⁹ P. Li, Y. Wang, F. Zeng, L. Chen, Z. Peng *et al.*, *Carbohydr. Res.*, **801**, 346 (2011).
- ³⁰ S. Mansouri, Y. Cuie, F. Winnik, Q. Shi, P. Lavigne *et al.*, *Biomaterials*, **2060**, 27 (2006).
- ³¹ A. Wan, Y. Sun and H. Li, *Int. J. Biol.*, **415**, 43 (2008).
- ³² S.-J. Yang, F.-H. Lin, K.-C. Tsai, M.-F. Wei, H.-M. Tsai *et al.*, *Bioconjugate Chem.*, **679**, 21 (2010).
- ³³ T. A. Sonia and C. P. Sharma, in “Oral Delivery of Insulin”, Elsevier, 2014, pp. 169-217.
- ³⁴ P. R. Vuddanda, V. M. Rajamanickam, M. Yaspal and S. Singh, *Biomed. Res. Int.*, **1**, 2014 (2014).
- ³⁵ N. Chekina, H. Horak, P. Jendelova, M. Trchova, M. J. Benes *et al.*, *J. Mater. Chem.*, **7630**, 21, (2011).
- ³⁶ C. Peniche, W. Arguelles-Monal, N. Davidenko, R. Sastre, A. Gallardo *et al.*, *Biomaterials*, **1869**, 20 (1999).
- ³⁷ A. Stoica-Guzun, L. Dobre, M. Stroescu and I. Jipa, *Analele Universitatii din Oradea Fascicula: Ecotoxicologie, Zootehnie si Tehnologii de Industrie Alimentara*, p. 1234 (2010).
- ³⁸ S. M. L. Silva, C. R. C. Braga, M. V. L. Fook, C. M. O. Raposo, L. H. Carvalho *et al.*, in “Infrared Spectroscopy-Materials Science, Engineering and Technology”, edited by T. Theophanides, InTech, 2012, pp. 43-62.
- ³⁹ K. Kh. Hammud, A. G. A. A. L. M. Raouf, R. R. Neama and M. Z. A. Rahman, *Diyala J. Pure Sci.*, **71**, 6 (2010).
- ⁴⁰ A. L. M. Raouf, K. K. Hammud, J. M. Mohammed and E. M. K. Al-Dulimy, *IJAPBC*, **773**, 3 (2014).
- ⁴¹ A. Noiri, V. Naponelli, J. F. Gregory III and A. D. Hanson, *Plant Physiol.*, **1101**, 143 (2007).
- ⁴² V. Georgieva, D. Zvezdova and L. Vlaev, *Chem. Cent. J.*, **1**, 6 (2012).
- ⁴³ W. Wang, C.-Y. Tong, X.-Y. Liu, T. Li, B. Liu *et al.*, *J. Cent. South Univ.*, **3311**, 22 (2015).
- ⁴⁴ G. Tataru, M. Popa and J. Desbrieres, *J. Hydrogels*, **70**, 1 (2015).
- ⁴⁵ N. Sarkar and I. J. Kim, in “Advanced Ceramic Processing”, edited by A. Mohamed, 2015, pp. 55-84.
- ⁴⁶ L. Ali, M. Ahmad and M. Usman, *Cellulose Chem. Technol.*, **49**, 143 (2015).
- ⁴⁷ P. L. Ritger and N. Peppas, *J. Control. Release*, **23**, 5 (1987).

⁴⁸ R. S. R. Murthy, in “Drug Delivery Nanoparticles Formulation and Characterization”, edited by Y. Pathak and D. Thassu, CRC Press, 2009, pp. 156-168.

⁴⁹ J. Xu, B. Xu, D. Shou, X. Xia and Y. Hu, *Polymers*, **7**, 1850 (2015).

⁵⁰ M. Uner, E. F. Karaman and Z. Aydogmus, *Trop. J. Pharm. Res.*, **653**, 13 (2014).

⁵¹ A. De, R. Bose, A. Kumar and S. Mozumdar, in “Targeted Delivery of Pesticides Using Biodegradable Polymeric Nanoparticles”, edited by A. De, R. Bose, A. Kumar and S. Mozumdar, Springer Science & Business Media, 2014, pp. 85-98.

⁵² ISO 10993-5:2009, Biomedical evaluation of medical devices, Part 5: Tests for *in vitro* cytotoxicity.

⁵³ M. A. Dobrovolskaia, J. D. Clogston, B. W. Neun, J. B. Hall, A. K. Patri *et al.*, *Nano Lett.*, **8**, 2180 (2008).

⁵⁴ D. W. Lee, K. Powers and R. Baney, *Carbohydr. Polym.*, **371**, 58 (2004).

⁵⁵ R. Nadesh, D. Narayanan, P. R. Sreerexha, S. Vadakumpully, U. Mony *et al.*, *J. Biomed. Mater. Res.*, **A**, 1 (2013).

⁵⁶ X. Li, Z. Yang, K. Yang, Y. Zhou, X. Chen *et al.*, *Nanoscale Res. Lett.*, **4**, 1502 (2009).